Modeling of underwater snake robots moving in a vertical plane in 3D

E. Kelasidi, K. Y. Pettersen and J. T. Gravdahl

Abstract— Increasing efficiency by improving the locomotion methods is a key issue for underwater robots. Consequently, an accurate dynamic model is important for both controller design and for the development of efficient locomotion methods. This paper presents a model of the kinematics and dynamics of an underwater snake robot moving in a vertical plane in 3D. The fluid contact forces (hydrodynamic forces) and torques (fluid moments) are modeled using analytical fluid dynamics. Hydrodynamic forces and torques, i.e. linear and nonlinear drag forces, current effects, added mass and fluid torque effects, are considered. In addition, this modeling approach also takes into account the hydrostatic forces (gravitational forces and buoyancy). The model is given in a closed form and is thus in a form that is well-suited for modern model-based control schemes. The proposed model is easily implemented and simulated, regardless of the number of robot links. Simulation results for lateral undulation and eel-like motion with a ten link robotic system are presented.

I. INTRODUCTION

For centuries, engineers and scientists have gained inspiration from the natural world, while searching for ideal solutions to technical problems. More recently, this process has been termed biomimetics. A significant research area in this field is snake robots, where several different models have been proposed [1]. Empirical and analytical studies of snake locomotion were reported by Gray [2], while among the first attempts to develop a snake prototype, the work of Hirose [3] is essential. An unambiguous result of all these studies is that the high number of DOFs of snake robots makes them difficult to control, but also gives them the ability to traverse irregular environments. Thus they can surpass the mobility of conventional wheeled, tracked or legged robots [1]. As an expansion of this field of interest, there has been increasing interest in the integration of robotic technology into underwater exploration, monitoring, and surveillance. Underwater snake robots carry a lot of potential for inspection of subsea oil and gas installations. Also, for he biological community and marine archeology, snake robots that are able to swim smoothly without much noise, and can traverse difficult environments like wrecks ship, are very interesting.

Comparing amphibious snake robots to the traditional ones, the former have the advantage of adaptability to aquatic environments. Research on amphibious snake robots (also referred to as lamprey robots or eel-like robots) is, however, much less extensive than for traditional types and fewer prototypes have been developed [4], [5], [6]. More recently, there has been growing interest in the design, modeling and control of underwater robots that propel themselves and maneuver by mimicking the movement of a fish. The dynamics of snake robots moving on land have been derived by various modeling techniques [1]. When it comes to swimming snake robots, only a few modeling approaches have been presented for eel-like robots [7], [8], [9].

Classical works by Taylor [10] and Lighthill [11] provide analytic models of fluid forces acting on the body during undulatory swimming. However, their analytic methods require a number of major simplifying assumptions. McIsaac and Ostrowski [7] present a dynamic model of anguilliform swimming for eel-like robots and Boyer et al. [8] present the dynamic modeling of a continuous three-dimensional swimming eel-like robot. Chen et al. [12] demonstrate a model for the body-fluid interaction in undulatory swimming of leeches, where the body is represented by a chain of rigid links and the hydrodynamic force model is based on resistive and reactive force theories. However, in all these works, the linear drag and the current effects are not taken into account, and no analytical expression for the fluid torques is derived. The linear drag and the current effects are both significant hydrodynamic effects that should be modeled to obtain a high level of accuracy for control design and analysis purposes [13]. In [14], the authors derive the equations of motion for a general multibody rectifier system taking into account the currents by assuming that the environmental force is a (possibly nonlinear) function of the relative velocity (i.e. the velocity of the link in water in the presence of current). However, the added mass and the fluid torque effects are not taken into account. [15] presents the modeling of the reactive force and moment acting on an elongated body moving in a weakly non-uniform potential flow. This model has been used to investigate the passive and the active swimming of a fish in a vortex street, while no viscous effects have been taken into account. In [16], a solution to the fast dynamics of eel-like robots has been proposed and tested on comparison with a Navier-Stokes solver.

It is worth mentioning that the majority of modeling results for underwater robots omit fluid moments (fluid torques) which are supposed to have a negligible effect on the overall motion of the system [7], [14], [17]. However, the fluid torques are directly related to the power consumption of the system (see e.g. [9]). The reason why they are neglected in these modeling approaches is probably in order to simplify

E. Kelasidi, and K. Y. Pettersen are with the Centre for Autonomous Marine Operations and Systems, Dept. of Engineering Cybernetics at NTNU, NO-7491 Trondheim, Norway. E-mail: {Eleni.Kelasidi,Kristin.Y.Pettersen}@itk.ntnu.no

J. T. Gravdahl is with the Dept. of Engineering Cybernetics at NTNU, NO-7491 Trondheim, Norway. E-mail: Tommy.Gravdahl@itk.ntnu.no

the hydrodynamic effects. It is also worth noting that, in [8], [9] and [18] fluid torques are modeled, but the drag force and torque are integrated numerically at each sample time of the algorithm and evaluated numerically. This results in the lack of a closed form solution. Furthermore, in [19], a simplified model of [14] is used to develop a feedback controller that achieves the desired body oscillation, orientation, and locomotion velocity.

In this paper we present a solution to the modeling problem that results in a closed form solution. Our approach considers hydrodynamic and hydrostatic forces and torques and avoids the numerical evaluation of drag effects. For control design purposes, it is a significant advantage that this hydrodynamic modeling concludes in a closed form, without the need of an algorithmic way to compute the drag force and torque. Thus it is well suited for model-based control design of the locomotion of underwater snake robots. It is well known that the hydrodynamic forces (fluid forces) induced by the motion of a rigid body in an underwater environment are very complex and highly nonlinear, and therefore several of these effects are often not taken into account when modeling the system. Our modeling approach, however, considers both linear and nonlinear drag forces (resistive fluid forces), the added mass effect (reactive fluid forces), the fluid moments and current effect. Furthermore, hydrostatic forces (gravitational and buoyancy forces) are considered, under the assumption that these forces are coincident.

To our best knowledge, this modeling approach is the first one that combines the hydrodynamic effects (i.e the current effect, the combination of linear and nonlinear drag effect, as derived in [13]), in analytical-closed form with the hydrostatic forces. It is important to notice that this model provides a complete closed form solution, which makes it possible to apply advanced control methods for underwater snake robots. In addition, our proposed modeling can be used by biologists to study creatures, such as leeches that swim by undulating the body like eels or snakes, except that the body oscillation occurs in a vertical (rather than horizontal) plane [12]. It is worth mentioning that this proposed modeling approach is valid for a neutrally buoyant underwater snake robot, moving in any tilted virtual 2D plane of 3D. Hence, an underwater snake robot model moving in the horizontal plane [13] is a special case of the developed snake robot model, achieved setting the hydrostatic forces to zero. The presented model is thus an extension of the underwater snake robot model moving in a virtual horizontal plane [13], and comprises underwater snake robots moving both in horizontal and vertical planes. In addition to providing completeness, this also makes the model applicable for unified control methods for underwater snake robots moving both in horizontal and vertical planes.

The paper is organized as follows. Section II presents a model of the kinematics and dynamics of the underwater snake robots, explaining in detail the hydrodynamic and hydrostatic effects. This is followed by simulation validations, for both serpentine and eel-like motions, in Section III. Conclusions and suggestions for future research are presented in Section IV.

II. MODELING OF UNDERWATER SNAKE ROBOTS

This section presents a continuous model of an underwater snake robot constrained to move within a vertical plane. The kinematics and dynamics of the robot will be presented taking into account the hydrodynamic and hydrostatic effects. It worth mentioning that the proposed modeling approach is valid for a neutrally buoyant underwater snake robot, moving in any tilted plane of 3D, as visualized in the Fig. 1.

A. Notations and defined symbols

The snake robot consists of n rigid links of equal length $2l, i = 1, \ldots, n$ interconnected by $n - 1$ joints. The links are assumed to have the same mass m and moment of inertia $J = \frac{1}{3}ml^2$. The mass of each link is uniformly distributed so that the link CM (center of mass) is located at its center point (at length l from the joint at each side). The total mass of the snake robot is therefore nm. In the following sections, the kinematics and dynamics of the robot will be modeled in terms of the mathematical symbols described in Table I and illustrated in Fig. 2. Vectors are either expressed in the global coordinate system or in the local link coordinate system of link i. This is indicated by the superscripts *global* or *link,i*, respectively. The following vectors and matrices are used in the development of the model

$$\mathbf{A} = \begin{bmatrix} 1 & 1 & & \\ & \ddots & \ddots & \\ & & 1 & 1 \end{bmatrix}, \mathbf{D} = \begin{bmatrix} 1 & -1 & & \\ & \ddots & \ddots & \\ & & 1 & -1 \end{bmatrix},$$

where $\mathbf{A}, \mathbf{D} \in \mathbb{R}^{(n-1) \times n}$. Furthermore,

$$\mathbf{e} = \begin{bmatrix} 1 & \ldots & 1 \end{bmatrix}^T \in \mathbb{R}^n, \mathbf{E} = \begin{bmatrix} \mathbf{e} & \mathbf{0}_{n \times 1} \\ \mathbf{0}_{n \times 1} & \mathbf{e} \end{bmatrix} \in \mathbb{R}^{2n \times 2},$$

$$\sin \theta = \begin{bmatrix} \sin \theta_1 & \ldots & \sin \theta_n \end{bmatrix}^T \in \mathbb{R}^n, \mathbf{S}_\theta = \mathrm{diag}(\sin \theta) \in \mathbb{R}^{n \times n},$$

$$\cos \theta = \begin{bmatrix} \cos \theta_1 & \ldots & \cos \theta_n \end{bmatrix}^T \in \mathbb{R}^n, \mathbf{C}_\theta = \mathrm{diag}(\cos \theta) \in \mathbb{R}^{n \times n},$$

$$\mathrm{sgn}\theta = \begin{bmatrix} \mathrm{sgn}\theta_1 & \ldots & \mathrm{sgn}\theta_n \end{bmatrix}^T \in \mathbb{R}^n$$

$$\dot{\theta}^2 = \begin{bmatrix} \dot{\theta}_1^2 & \ldots & \dot{\theta}_n^2 \end{bmatrix}^T \in \mathbb{R}^n, \mathbf{J} = J\mathbf{I}_n, \mathbf{L} = l\mathbf{I}_n, \mathbf{M} = m\mathbf{I}_n$$

$$\mathbf{K} = \mathbf{A}^T (\mathbf{D}\mathbf{D}^T)^{-1} \mathbf{D}, \mathbf{V} = \mathbf{A}^T (\mathbf{D}\mathbf{D}^T)^{-1} \mathbf{A}$$

Matrices $\mathbf{A}$ and $\mathbf{D}$ represent, respectively, an addition and a difference matrix, while vector $\mathbf{e}$ represents a summation vector (see, e.g. [1]).

TABLE I: Parameters notation of the underwater snake robot

Symbol	Description	Vector
n	The number of links	
l	The half length of a link	
m	Mass of each link	
J	Moment of inertia of each link	
θ_i	Angle between link i and the global z axis	$\theta \in \mathbb{R}^n$
ϕ_i	Angle of joint i	$\phi \in \mathbb{R}^{n-1}$
(y_i, z_i)	Global coordinates of the CM of link i	$\mathbf{Y}, \mathbf{Z} \in \mathbb{R}^n$
(p_y, p_z)	Global coordinates of the CM of the robot	$\mathbf{p}_{CM} \in \mathbb{R}^2$
u_i	Actuator torque of joint between link i and link $i+1$	$\mathbf{u} \in \mathbb{R}^{n-1}$
u_{i-1}	Actuator torque of joint between link i and link $i-1$	$\mathbf{u} \in \mathbb{R}^{n-1}$
$(f_{y,i}, f_{z,i})$	Fluid force on link i	$\mathbf{f}_y, \mathbf{f}_z \in \mathbb{R}^n$
$f_{w,i}$	Gravitational force on link i	$\mathbf{f}_w \in \mathbb{R}^n$
$f_{b,i}$	Buoyancy force on link i	$\mathbf{f}_b \in \mathbb{R}^n$
τ_i	Fluid torque on link i	$\tau \in \mathbb{R}^n$
$(h_{y,i}, h_{z,i})$	Joint constraint force on link i from link $i+1$	$\mathbf{h}_y, \mathbf{h}_z \in \mathbb{R}^{n-1}$
$-(h_{y,i-1}, h_{z,i-1})$	Joint constraint force on link i from link $i-1$	$\mathbf{h}_y, \mathbf{h}_z \in \mathbb{R}^{n-1}$

B. Kinematics of the underwater snake robot

The kinematics of an underwater snake robot moving in a virtual vertical plane is similar to that of an underwater snake robot moving in a virtual horizontal plane. In this
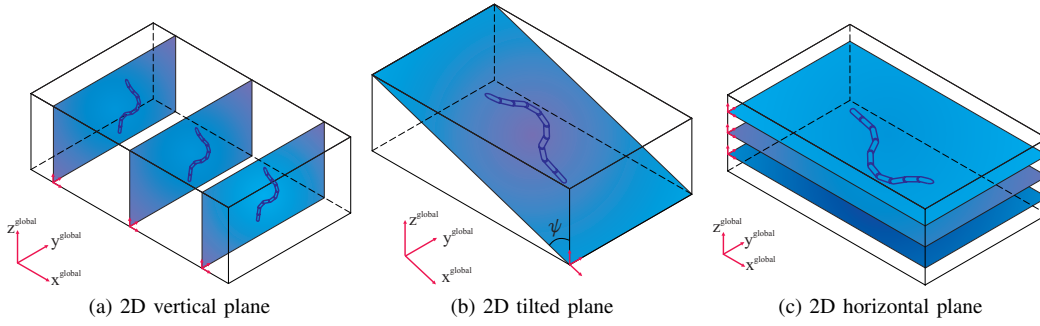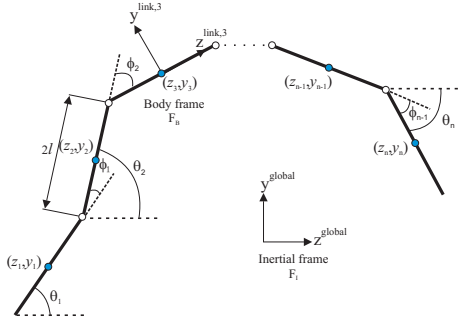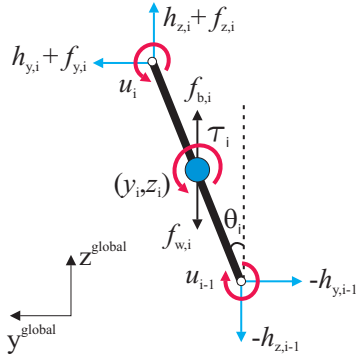
Fig. 1: Visualization of a ten link underwater snake robot motion in any 2D subspace

(a) Kinematic parameters

(b) Forces and torques acting on each link

Fig. 2: Underwater snake robot

section we provide a brief presentation of the kinematics for completeness. An extensive presentation of the snake robot kinematics can be found in [13]. The snake robot is assumed to move in a virtual vertical plane, fully immersed in water, and has $n+2$ degrees of freedom (n link angles and the y-z position of the robot). The *link angle* of each link $i \in 1, \ldots, n$ of the snake robot is denoted by $\theta_i \in \mathbb{R}$ and is defined as the angle that the link forms with the global z axis with counterclockwise positive direction, while the *joint angle* of joint $i \in 1, \ldots, n-1$ is denoted $\phi_i \in \mathbb{R}$ and defined as

$$\phi_i = \theta_i - \theta_{i-1}. \tag{1}$$

The link angles and the joint angles are assembled in the vectors $\boldsymbol{\theta} = [\theta_1, \ldots, \theta_n]^T \in \mathbb{R}^n$ and $\boldsymbol{\phi} = [\phi_1, \ldots, \phi_{n-1}]^T \in \mathbb{R}^{n-1}$, respectively. The *heading* (or *orientation*) $\bar{\theta} \in \mathbb{R}$ of the snake is defined as the average of the link angles as is similar for land-based snake robots in [1]

$$\bar{\theta} = \frac{1}{n} \sum_{i=1}^{n} \theta_i. \tag{2}$$

The model of the snake robot will be derived using link angles to simplify the mathematical expressions. The local coordinate system of each link is fixed in the CM of the link

with y (normal) and z (tangential) axes oriented such that they are aligned with the global y and z axis, respectively, when all the link angles are zero. The rotation matrix from the global frame to the frame of link i is

$$\mathbf{R}_{\mathrm{link},i}^{\mathrm{global}} = \begin{bmatrix} \cos \theta_i & \sin \theta_i \\ -\sin \theta_i & \cos \theta_i \end{bmatrix}. \tag{3}$$

The global frame position $\mathbf{p}_{\mathrm{CM}} \in \mathbb{R}^2$ of the CM of the robot is given by

$$\mathbf{p}_{\mathrm{CM}} = \begin{bmatrix} p_y \\ p_z \end{bmatrix} = \begin{bmatrix} \frac{1}{nm} \sum_{i=1}^{n} m y_i \\ \frac{1}{nm} \sum_{i=1}^{n} m z_i \end{bmatrix} = \frac{1}{n} \begin{bmatrix} \mathbf{e}^T \mathbf{Y} \\ \mathbf{e}^T \mathbf{Z} \end{bmatrix}, \tag{4}$$

where (y_i, z_i) are the global frame coordinates of the CM of link i, $\mathbf{Y} = [y_1, \ldots, y_n]^T \in \mathbb{R}^n$ and $\mathbf{Z} = [z_1, \ldots, z_n]^T \in \mathbb{R}^n$. The forward velocity of the robot is denoted by $\bar{v}_t \in \mathbb{R}$ and is defined as the component of the CM velocity along the current heading of the snake, i.e.

$$\bar{v}_t = \dot{p}_y \sin \bar{\theta} + \dot{p}_z \cos \bar{\theta}. \tag{5}$$

The links are constrained by the joints according to

$$\mathbf{DY} + l\mathbf{A} \sin \theta = \mathbf{0}, \quad \mathbf{DZ} + l\mathbf{A} \cos \theta = \mathbf{0}. \tag{6}$$

The position of the individual links as a function of the CM position and the link angles of the robot can be expressed as

$$\mathbf{Y} = -l\mathbf{K}^T \sin \theta + \mathbf{e} p_y, \quad \mathbf{Z} = -l\mathbf{K}^T \cos \theta + \mathbf{e} p_z, \tag{7}$$

where $\mathbf{K} = \mathbf{A}^T \left(\mathbf{D}\mathbf{D}^T \right)^{-1} \mathbf{D} \in \mathbb{R}^{n \times n}$, and where $\mathbf{D}\mathbf{D}^T$ is non-singular and thereby invertible [1]. The linear velocities of the links are found by differentiating the position of the individual links (7) with respect to time, which gives

$$\dot{\mathbf{Y}} = -l\mathbf{K}^T \mathbf{C}_\theta \dot{\theta} + \mathbf{e} \dot{p}_y, \quad \dot{\mathbf{Z}} = l\mathbf{K}^T \mathbf{S}_\theta \dot{\theta} + \mathbf{e} \dot{p}_z. \tag{8}$$

The linear accelerations of the links are found by differentiating the velocity of the individual links (8) with respect to time, which gives

$$\ddot{\mathbf{Y}} = l\mathbf{K}^T \left(\mathbf{S}_\theta \dot{\theta}^2 - \mathbf{C}_\theta \ddot{\theta} \right) + \mathbf{e} \ddot{p}_y, \quad \ddot{\mathbf{Z}} = l\mathbf{K}^T \left(\mathbf{C}_\theta \dot{\theta}^2 + \mathbf{S}_\theta \ddot{\theta} \right) + \mathbf{e} \ddot{p}_z. \tag{9}$$

Note that in this paper (9) has been adjusted compared to the corresponding expression presented in [13] in order to express the acceleration of the links in a more proper way, by also taking into account the acceleration of the CM.

C. Hydrodynamic modeling

The hydrodynamics of an underwater snake robot moving in virtual vertical plane is similar to that of an underwater snake robot moving in a virtual horizontal plane, except that the motion is performed in the $y-z$ plane instead of the $x-y$ plane. In this section we provide a brief presentation of the hydrodynamic for completeness. An extensive presentation of the snake robot hydrodynamics can be found in [13].

As it is pointed in the bio-robotics community, for swimming robots, the dynamic modeling of the contact forces is most complicated compared to the modeling of the overall

rigid motion and the dynamics of the body deformation. For large anguilliform swimmers and hyper-redundant mechanisms, it is necessary to take into account the resistive and reactive forces (see, e.g. [13]). Thus, both added mass and drag effects need to be modeled. The Navier-Stokes equations can be used in order to model the full hydrodynamic effects for swimming vehicles. However, it is very difficult to solve these equations and they are quite unsuited for robotics control design purposes. It is worth mentioning that for control design purposes, it is important to model the hydrodynamic phenomena in a sufficiently simple manner while taking into account all the hydrodynamic effects that are significant for the control design. Hence, the modeling for control design purposes poses different challenges than hydrodynamic modeling for simulations [13].

In the modeling approach presented in this paper, each link of the underwater snake robot is considered as an isolated segment. Each segment is approximated as an elliptical cylinder and the fluid forces are modeled using Morison's equations [20] and assuming that the robot is a slender body. In particular, the fluid forces are modeled in each cross section of the links and depends only on the motion the transverse link. We now present some assumptions underlying our modeling approach.

Assumption 1. The fluid is viscid, incompressible, and irrotational in the inertia frame.

Assumption 2. The current in the inertial frame, $v_c = [V_{y,i}, V_{z,i}]^T$, is constant and irrotational.

Remark 1. Assumption 1 is a common assumption in hydrodynamic modeling of slender body swimming robots [8], [9], [21], while Assumption 2 is a reasonable simplification of the real-world situation [22],[23].

The fluid forces are functions of the current and it is shown in the hydrodynamics literature, see e.g. [23], that the force exerted by the current can be characterized by the current velocity vector. This vector can be added vectorially to the link speed before calculating the fluid forces. Hence, the fluid forces will be expressed as functions of relative velocity, and the relative velocity of link i is defined as $v_{r,i}^{\text{link},i} = \dot{p}_i^{\text{link},i} - v_{c,i}^{\text{link},i}$ [23], where $v_{c,i}^{\text{link},i} = (\mathbf{R}_{\text{link},i}^{\text{global}})^T v_c = [v_{y,i}, v_{z,i}]^T$ is the current velocity expressed in body frame coordinates (F_B) and $v_c = [V_{y,i}, V_{z,i}]^T$ is the current velocity expressed in inertial frame coordinates (F_I). Due to Assumption 2 $\dot{v}_c = 0$ and thus

$$\dot{v}_{c,i}^{\text{link},i} = \frac{d}{dt}\left((\mathbf{R}_{\text{link},i}^{\text{global}})^T v_c\right) = \begin{bmatrix} -\sin\theta_i\dot{\theta}_i & -\cos\theta_i\dot{\theta}_i \\ \cos\theta_i\dot{\theta}_i & -\sin\theta_i\dot{\theta}_i \end{bmatrix} \begin{bmatrix} V_{y,i} \\ V_{z,i} \end{bmatrix} \quad (10)$$

As described by [9],[21], each link is subject to a force from the fluid acting on the CM of the link and also a fluid torque acting on the CM. In the following, we will derive the fluid forces and torques acting on the snake robot, using Morison's equations [20]. In particular, we will first state the assumption on which the development is based, then present how the force exerted by the fluid on a cylindrical object is made up of two components: the virtual mass force (added mass effect) and the drag force. The drag model that is employed here is in a form which takes into account the

generalized case of anisotropic friction acting on each link. In particular, this means that each link has two drag coefficients, c_n and c_t, describing the drag force in the normal (along link y axis) and tangential (along link z axis) direction of the link, respectively. The fluid forces exerted on link i by the fluid can then be expressed as [20], [21]

$$f_i^{\text{link},i} = -\hat{\mathbf{C}}_A \dot{v}_{r,i}^{\text{link},i} - \hat{\mathbf{C}}_D v_{r,i}^{\text{link},i} - \hat{\mathbf{C}}_D \,\text{sgn}\left(v_{r,i}^{\text{link},i}\right)\left(v_{r,i}^{\text{link},i}\right)^2, \quad (11)$$

where $\dot{v}_{r,i}^{\text{link},i} = \ddot{p}_i^{\text{link},i} - \dot{v}_{c,i}^{\text{link},i}$ is the relative acceleration of link i, $\dot{p}_i^{\text{link},i}$ and $\ddot{p}_i^{\text{link},i}$ are the velocity and the acceleration of link i, respectively, expressed in the body frame, and $\hat{\mathbf{C}}_A$ and $\hat{\mathbf{C}}_D$ are constant diagonal (2×2) matrices depending on the shape of the body and the fluid characteristics.

In [13], it is shown that for the cylindrical links with major diameter $2a$ and minor diameter $2b$ and taking into account that the length of each link is $2l$, $\hat{\mathbf{C}}_D$, $\hat{\mathbf{C}}_A$ are expressed as

$$\hat{\mathbf{C}}_D = \begin{bmatrix} c_n & 0 \\ 0 & c_t \end{bmatrix} = \begin{bmatrix} \frac{1}{2}\rho C_D 2a2l & 0 \\ 0 & \frac{1}{2}\rho\pi C_f \frac{(b+a)}{2}2l \end{bmatrix}, \quad (12)$$

$$\hat{\mathbf{C}}_A = \begin{bmatrix} \mu_n & 0 \\ 0 & \mu_t \end{bmatrix} = \begin{bmatrix} \rho\pi C_A a^2 2l & 0 \\ 0 & 0 \end{bmatrix}, \quad (13)$$

where C_D and C_f are the drag coefficients in the y and z directions of motion, while C_A denotes the added mass coefficient [5], [24] and ρ is the density of the fluid. The added mass parameter in the z direction is considered equal to zero ($\mu_t = 0$), because the added mass of a slender body in the longitudinal direction can be neglected compared to the body mass [24].

After modeling the fluid forces acting on the snake robot, we will now model the fluid moment τ_i. Many previous studies of multi-link swimmers neglect fluid moments as they are assumed to have little effect on the overall motion of the system [7], [17]. In [9] a finite segment approach is employed in order to take into account the fluid moments, however, in this modeling approach the drag moment is evaluated numerically. Additionally, in [8] and [18] the fluid moments are taken into account but concluded in an algorithmic approach of computing the drag moment. We decide to include the fluid moments in the model because, first of all, this implies a more accurate modeling approach from a hydrodynamic perspective and, second, due to the fact that the fluid moments are directly related to the power consumption of the system. Since the fluid torques contribute significantly to the required actuation torques at the joints [9] and as the research on underwater swimming robots is expanding, there is an increased demand for improved efficiency to allow for longer missions to be undertaken.

The fluid torque is a result of the link rotation only and thus the fluid torque on the CM of link i is a result of fluid forces acting normal to the link during link rotation. In [13] it is shown that the torque applied on link i by the fluid can be modeled through the relation

$$\tau_i = -\lambda_1 \ddot{\theta}_i - \lambda_2 \dot{\theta}_i - \lambda_3 \dot{\theta}_i|\dot{\theta}_i|, \quad (14)$$

where the λ_1, λ_2 and λ_3 parameters depend on the shape of the body and the fluid characteristics. We will now derive

the fluid force parameters λ_1, λ_2 and λ_3. It is well-known that, for a cylinder, the added mass torque reduces to a simple analytic form with the parameter λ_1 expressed for a link with length $2l$ as [9], [21], [24]

$$\lambda_1 = \frac{1}{12} \rho \pi C_M (a^2 - b^2)^2 l^3, \tag{15}$$

where C_M is the added inertia coefficient. Additionally, the total drag torque on link i is given by [13]

$$\tau_{drag} = -\lambda_2 \dot{\theta}_i - \lambda_3 \dot{\theta}_i |\dot{\theta}_i| \tag{16}$$

where λ_2 and λ_3 are given by

$$\lambda_2 = \frac{1}{6} \rho \pi C_f (a+b) l^3 \text{ and } \lambda_3 = \frac{1}{8} \rho \pi C_f (a+b) l^4 \tag{17}$$

The matrix $\hat{\mathbf{C}}_D$ and the parameters λ_2, λ_3 represent the drag force parameters due to the pressure difference between the two sides of the body, while $\hat{\mathbf{C}}_A$ and λ_1 stand for the added mass of fluid carried by the moving body. We now present the expression for the global frame fluid forces on link i. Using the rotation matrix (3) we can express the global frame fluid forces on link i as:

$$f_i^{\text{global}} = \mathbf{R}_{\text{link},i}^{\text{global}} f^{\text{link},i} = \begin{bmatrix} \cos\theta_i & \sin\theta_i \\ -\sin\theta_i & \cos\theta_i \end{bmatrix} \begin{bmatrix} f_{y,i}^{\text{link},i} \\ f_{z,i}^{\text{link},i} \end{bmatrix}$$

$$= -\mathbf{R}_{\text{link},i}^{\text{global}} \hat{\mathbf{C}}_A \left((\mathbf{R}_{\text{link},i}^{\text{global}})^T \begin{bmatrix} \ddot{y}_i \\ \ddot{z}_i \end{bmatrix} - \begin{bmatrix} -\sin\theta_i \dot{\theta}_i & -\cos\theta_i \dot{\theta}_i \\ \cos\theta_i \dot{\theta}_i & -\sin\theta_i \dot{\theta}_i \end{bmatrix} \begin{bmatrix} V_{y,i} \\ V_{z,i} \end{bmatrix} \right)$$

$$- \mathbf{R}_{\text{link},i}^{\text{global}} \hat{\mathbf{C}}_D (\mathbf{R}_{\text{link},i}^{\text{global}})^T \begin{bmatrix} \dot{y}_i - V_{y,i} \\ \dot{z}_i - V_{z,i} \end{bmatrix} - \mathbf{R}_{\text{link},i}^{\text{global}} \hat{\mathbf{C}}_D \text{sgn}\left(\begin{bmatrix} V_{ry,i} \\ V_{rz,i} \end{bmatrix} \right) \begin{bmatrix} V_{ry,i}^2 \\ V_{rz,i}^2 \end{bmatrix} \tag{18}$$

where

$$\begin{bmatrix} V_{ry,i} \\ V_{rz,i} \end{bmatrix} = (\mathbf{R}_{\text{link},i}^{\text{global}})^T \begin{bmatrix} \dot{y}_i - V_{y,i} \\ \dot{z}_i - V_{z,i} \end{bmatrix}. \tag{19}$$

By performing the matrix multiplications and assembling the forces on all links in vector form, we can rewrite the global frame fluid forces on the links as

$$\mathbf{f} = \begin{bmatrix} \mathbf{f}_y \\ \mathbf{f}_z \end{bmatrix} = \begin{bmatrix} \mathbf{f}_{A_y} \\ \mathbf{f}_{A_z} \end{bmatrix} + \begin{bmatrix} \mathbf{f}_{D_y}^I \\ \mathbf{f}_{D_z}^I \end{bmatrix} + \begin{bmatrix} \mathbf{f}_{D_y}^{II} \\ \mathbf{f}_{D_z}^{II} \end{bmatrix}, \tag{20}$$

where $\mathbf{f}_{A_y}$ and $\mathbf{f}_{A_z}$ represent the effects from added mass forces and are expressed as

$$\begin{bmatrix} \mathbf{f}_{A_y} \\ \mathbf{f}_{A_z} \end{bmatrix} = - \begin{bmatrix} \mu_n (\mathbf{C}_\theta)^2 & -\mu_n \mathbf{S}_\theta \mathbf{C}_\theta \\ -\mu_n \mathbf{S}_\theta \mathbf{C}_\theta & \mu_n (\mathbf{S}_\theta)^2 \end{bmatrix} \begin{bmatrix} \ddot{\mathbf{Y}} \\ \ddot{\mathbf{Z}} \end{bmatrix}$$
$$- \begin{bmatrix} \mu_n \mathbf{S}_\theta \mathbf{C}_\theta & \mu_n (\mathbf{C}_\theta)^2 \\ -\mu_n (\mathbf{S}_\theta)^2 & -\mu_n \mathbf{S}_\theta \mathbf{C}_\theta \end{bmatrix} \begin{bmatrix} \mathbf{V}_y^a \\ \mathbf{V}_z^a \end{bmatrix} \dot{\theta}, \tag{21}$$

where $\mathbf{V}_y^a = \text{diag}(V_{y,1}, \dots, V_{y,n}) \in \mathbb{R}^{n \times n}$ and $\mathbf{V}_z^a = \text{diag}(V_{z,1}, \dots, V_{z,n}) \in \mathbb{R}^{n \times n}$. The vectors $\mathbf{f}_{D_y}^I$, $\mathbf{f}_{D_z}^I$ and $\mathbf{f}_{D_y}^{II}$, $\mathbf{f}_{D_z}^{II}$ present the effects from the linear (22) and nonlinear drag forces (23), respectively, where the relative velocities are given from the Eq. 24.

$$\begin{bmatrix} \mathbf{f}_{D_y}^I \\ \mathbf{f}_{D_z}^I \end{bmatrix} = - \begin{bmatrix} c_t (\mathbf{S}_\theta)^2 + c_n (\mathbf{C}_\theta)^2 & (c_t - c_n) \mathbf{S}_\theta \mathbf{C}_\theta \\ (c_t - c_n) \mathbf{S}_\theta \mathbf{C}_\theta & c_t (\mathbf{C}_\theta)^2 + c_n (\mathbf{S}_\theta)^2 \end{bmatrix} \begin{bmatrix} \dot{\mathbf{Y}} - \mathbf{V}_y \\ \dot{\mathbf{Z}} - \mathbf{V}_z \end{bmatrix} \tag{22}$$

$$\begin{bmatrix} \mathbf{f}_{D_y}^{II} \\ \mathbf{f}_{D_z}^{II} \end{bmatrix} = - \begin{bmatrix} c_n \mathbf{C}_\theta & c_t \mathbf{S}_\theta \\ -c_n \mathbf{S}_\theta & c_t \mathbf{C}_\theta \end{bmatrix} \text{sgn}\left(\begin{bmatrix} \mathbf{V}_{r_y} \\ \mathbf{V}_{r_z} \end{bmatrix} \right) \begin{bmatrix} \mathbf{V}_{r_y}^2 \\ \mathbf{V}_{r_z}^2 \end{bmatrix} \tag{23}$$

$$\begin{bmatrix} \mathbf{V}_{r_y} \\ \mathbf{V}_{r_z} \end{bmatrix} = \begin{bmatrix} \mathbf{C}_\theta & -\mathbf{S}_\theta \\ \mathbf{S}_\theta & \mathbf{C}_\theta \end{bmatrix} \begin{bmatrix} \dot{\mathbf{Y}} - \mathbf{V}_y \\ \dot{\mathbf{Z}} - \mathbf{V}_z \end{bmatrix} \tag{24}$$

In addition, the fluid torques on all links in matrix form are

$$\tau = -\Lambda_1 \ddot{\theta} - \Lambda_2 \dot{\theta} - \Lambda_3 \dot{\theta} |\dot{\theta}|, \tag{25}$$

where $\Lambda_1 = \lambda_1 \mathbf{I}_n$, $\Lambda_2 = \lambda_2 \mathbf{I}_n$ and $\Lambda_3 = \lambda_3 \mathbf{I}_n$.

D. Hydrostatic forces

It is well-known that for an elliptical cylinder with uniformly mass distribution the center of gravity is the geometrical center of the cylinder [25]. Furthermore, the center of buoyancy is located at the center of the volume of an object, which means that for the cylindrical joint the center of buoyancy is coincident with the center of gravity. Thus, we will consider the following assumption is our modeling approach.

Assumption 3. The snake robot is considered not neutrally buoyant, while the center of gravity and the center of buoyancy are coincident. Since the center of gravity and buoyancy are coincident, the total moment due to the hydrostatic forces vanishes.

Remark 2. Assumption 3 is a reasonable assumption for any symmetric object with uniformly mass distribution, i.e for a homogeneous symmetric body, the center of buoyancy and center of mass are equivalent [25].

As pointed out in Assumption 3, the center of gravity, (y_{g_i}, z_{g_i}) and center of buoyancy, (y_{b_i}, z_{b_i}) coincide in each joint of the robot, i.e $(y_i, z_i) = (y_{g_i}, z_{g_i}) = (y_{b_i}, z_{b_i})$. Using Eq. (4), it is obvious that the center of gravity and buoyancy of the snake also coincide, even if the center of the robot oscillates during the locomotion of the snake robot.

The hydrostatic forces are illustrated in Fig. 3 for the case of a tilted (inclined) plane (Fig. 1b). Since the forces due to the gravity and buoyancy are neither parallel nor perpendicular to the inclined plane, it is imperative that it be resolved into two components of force which are directed parallel and perpendicular to the incline, shown in Fig. 1b. Without loss of generality, in this paper we consider the case where the tilted plane angle is $\psi = 0$ (i.e. locomotion in vertical 2D plane of 3D).
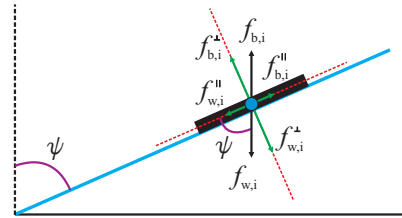

Fig. 3: Hydrostatic forces

Remark 3. The hydrostatic forces and torques vanish for a neutrally buoyant underwater snake robot, leading to the conclusion that the proposed modeling approach is valid for underwater motion in any 2D-tilted plane of 3D. However, in this paper the hydrostatic forces are analysed for the tilted plane angle $\psi = 0$ under the Assumption 3, in order to investigate the results in locomotion of a not neutrally buoyant snake robot.

Gravity forces act at the center of gravity of each link in the system. The force due to gravity acting on an arbitrary link i is given by:

$$f_{w,i} = -mg = -\rho_b V g, \tag{26}$$

where, ρ_b is the density of the joint, g is the acceleration of gravity and V is the volume of fluid displaced by link i. By assembling the forces on all links in vector form, we can rewrite the global frame gravity forces on the links as

$$\mathbf{f_w} = [f_{w,1}, f_{w,2}, \ldots, f_{w,n}]^T, \qquad (27)$$

The buoyancy force is proportional to the mass of the fluid displaced by the link, it acts through the center of gravity of the link and is given by the expression:

$$f_{b,i} = \rho V g, \qquad (28)$$

where, ρ is the density of the fluid. Eq. (29) gives the sum of the hydrostatic forces in each joint.

$$f_{b,i} + f_{w,i} = \rho V g - \rho_b V g = m(\frac{\rho}{\rho_b} - 1)g. \qquad (29)$$

By assembling the forces on all links in vector form, we can rewrite the global frame buoyancy forces on the links as

$$\mathbf{f_b} = [f_{b,1}, f_{b,2}, \ldots, f_{b,n}]^T, \qquad (30)$$

Remark 4. It is worth mentioning that if $\rho = \rho_b$ then the robot is neutrally buoyant, if $\rho > \rho_b$ the robot will float and if $\rho < \rho_b$ the robot will sink [25], [26].

E. Equations of motion

This section presents the equations of motion for the underwater snake robot. The forces and torques acting on link i are visualized in Fig. 2b and the force balance for link i in global frame coordinates is given by

$$m\ddot{y}_i = h_{y,i} - h_{y,i-1} + f_{y,i}, \quad m\ddot{z}_i = h_{z,i} - h_{z,i-1} + f_{z,i} + f_{b,i} + f_{w,i} \qquad (31)$$

The force balance equations for all links may be expressed in matrix form as

$$m\ddot{\mathbf{Y}} = \mathbf{D}^T \mathbf{h_y} + \mathbf{f_y}, \quad m\ddot{\mathbf{Z}} = \mathbf{D}^T \mathbf{h_z} + \mathbf{f_z} + \mathbf{f_b} + \mathbf{f_w}. \qquad (32)$$

Note that the link accelerations may also be expressed by differentiating (6) twice with respect to time. This gives

$$\mathbf{D}\ddot{\mathbf{Y}} = l\mathbf{A}\left(\mathbf{S}_\theta \dot{\theta}^2 - \mathbf{C}_\theta \ddot{\theta}\right), \quad \mathbf{D}\ddot{\mathbf{Z}} = l\mathbf{A}\left(\mathbf{C}_\theta \dot{\theta}^2 + \mathbf{S}_\theta \ddot{\theta}\right). \qquad (33)$$

We obtain the acceleration of the CM by differentiating (4) twice with respect to time, inserting (32), and noting that the constraint forces $\mathbf{h}_y$ and $\mathbf{h}_z$, are cancelled out when the link accelerations are summed. This gives

$$\begin{bmatrix} \ddot{p}_y \\ \ddot{p}_z \end{bmatrix} = \frac{1}{n} \begin{bmatrix} \mathbf{e}^T \ddot{\mathbf{Y}} \\ \mathbf{e}^T \ddot{\mathbf{Z}} \end{bmatrix} = \frac{1}{nm} \begin{bmatrix} \mathbf{e}^T & \mathbf{0}_{1 \times n} \\ \mathbf{0}_{1 \times n} & \mathbf{e}^T \end{bmatrix} \mathbf{f} + \frac{1}{nm} \begin{bmatrix} 0 \\ \mathbf{e}^T(\mathbf{f_b} + \mathbf{f_w}) \end{bmatrix} \qquad (34)$$

By inserting (9), (20) and (21) into (34) the acceleration of the CM may be expressed as

$$\begin{bmatrix} \ddot{p}_y \\ \ddot{p}_z \end{bmatrix} = -\mathbf{M}_p \begin{bmatrix} \mathbf{e}^T \mu_n \mathbf{C}_\theta^2 & -\mathbf{e}^T \mu_n \mathbf{S}_\theta \mathbf{C}_\theta \\ -\mathbf{e}^T \mu_n \mathbf{S}_\theta \mathbf{C}_\theta & \mathbf{e}^T \mu_n \mathbf{S}_\theta^2 \end{bmatrix} \begin{bmatrix} l\mathbf{K}^T(\mathbf{S}_\theta \dot{\theta}^2 - \mathbf{C}_\theta \ddot{\theta}) \\ l\mathbf{K}^T(\mathbf{C}_\theta \dot{\theta}^2 + \mathbf{S}_\theta \ddot{\theta}) \end{bmatrix}$$
$$-\mathbf{M}_p \begin{bmatrix} \mathbf{e}^T \mu_n \mathbf{S}_\theta \mathbf{C}_\theta & \mathbf{e}^T \mu_n \mathbf{C}_\theta^2 \\ -\mathbf{e}^T \mu_n \mathbf{S}_\theta^2 & -\mathbf{e}^T \mu_n \mathbf{S}_\theta \mathbf{C}_\theta \end{bmatrix} \begin{bmatrix} \mathbf{V}_y^a \\ \mathbf{V}_z^a \end{bmatrix} \dot{\theta}$$
$$+\mathbf{M}_p \begin{bmatrix} \mathbf{e}^T \mathbf{f_{Dy}} \\ \mathbf{e}^T \mathbf{f_{Dz}} \end{bmatrix} + \mathbf{M}_p \begin{bmatrix} 0 \\ \mathbf{e}^T(\mathbf{f_b} + \mathbf{f_w}) \end{bmatrix}$$

where $\qquad (35)$

$$\mathbf{M}_p = \begin{bmatrix} m_{11} & m_{12} \\ m_{21} & m_{22} \end{bmatrix} = \begin{bmatrix} nm + \mathbf{e}^T \mu_n \mathbf{C}_\theta^2 \mathbf{e} & -\mathbf{e}^T \mu_n \mathbf{S}_\theta \mathbf{C}_\theta \mathbf{e} \\ -\mathbf{e}^T \mu_n \mathbf{S}_\theta \mathbf{C}_\theta \mathbf{e} & nm + \mathbf{e}^T \mu_n \mathbf{S}_\theta^2 \mathbf{e} \end{bmatrix}^{-1}. \qquad (36)$$

and $\mathbf{f_{Dy}} = \mathbf{f_{D_y}^I} + \mathbf{f_{D_y}^{II}}$ and $\mathbf{f_{Dz}} = \mathbf{f_{D_z}^I} + \mathbf{f_{D_z}^{II}}$ are the drag forces in y and z directions. Additionally, it is easily verifiable that the determinant $n^2 m^2 + nm\mu_n + \mu_n^2 \sum_{i=1}^{n-1} \sum_{j=i+1}^{n} (\sin(\theta_i - \theta_j))^2$ is nonzero for $n \neq 0$ and $m \neq 0$.

The torque balance for link i is given by

$$J\ddot{\theta}_i = u_i - u_{i-1} - l\sin\theta_i\left(h'_{z,i} + h'_{z,i-1}\right) + l\cos\theta_i\left(h_{y,i} + h_{y,i-1}\right) + \tau_i, \qquad (37)$$

where $h'_{z,i} + h'_{z,i-1}$ is the joint constraint forces which contribute in the torque balance equation (the hydrostatic forces act in the center of gravity and thus the torques due to the gravity and buoyancy are removed). Hence, the torque balance equations for all links may be expressed in matrix form as

$$\mathbf{J}\ddot{\theta} = \mathbf{D}^T \mathbf{u} - l\mathbf{S}_\theta \mathbf{A}^T \mathbf{h}'_z + l\mathbf{C}_\theta \mathbf{A}^T \mathbf{h}_y + \tau, \qquad (38)$$

where τ is given from (25). What now remains is to remove the constraint forces from (38). Premultiplying (32) by $\mathbf{D}$ and solving for $\mathbf{h}_y$ and $\mathbf{h}'_z$, we can write the expression for the joint constraint forces as

$$\mathbf{h}_y = (\mathbf{DD}^T)^{-1} \mathbf{D}(m\ddot{\mathbf{Y}} - \mu_n \mathbf{S}_\theta \mathbf{C}_\theta \ddot{\mathbf{Z}} + \mu_n (\mathbf{C}_\theta)^2 \ddot{\mathbf{Y}}$$
$$+ \mu_n (\mathbf{C}_\theta)^2 \mathbf{V}_z^a \dot{\theta} + \mu_n \mathbf{S}_\theta \mathbf{C}_\theta \mathbf{V}_y^a \dot{\theta} - \mathbf{f_{D_y}^I} - \mathbf{f_{D_y}^{II}}). \qquad (39)$$

$$\mathbf{h}'_z = (\mathbf{DD}^T)^{-1} \mathbf{D}(m\ddot{\mathbf{Z}} + \mu_n (\mathbf{S}_\theta)^2 \ddot{\mathbf{Z}} - \mu_n \mathbf{S}_\theta \mathbf{C}_\theta \ddot{\mathbf{Y}}$$
$$- \mu_n \mathbf{S}_\theta \mathbf{C}_\theta \mathbf{V}_z^a \dot{\theta} - \mu_n (\mathbf{S}_\theta)^2 \mathbf{V}_y^a \dot{\theta} - \mathbf{f_{D_z}^I} - \mathbf{f_{D_z}^{II}}) \qquad (40)$$

Inserting in (38) the joint constraints forces (39, 40) and also replacing $\mathbf{D}\ddot{\mathbf{Y}}$, $\mathbf{D}\ddot{\mathbf{Z}}$ with (33), $\ddot{\mathbf{Y}}$, $\ddot{\mathbf{Z}}$ with (9) and $\ddot{p}_y$, $\ddot{p}_z$ with (35), we can finally express the model of the robot as

$$\mathbf{M}_\theta \ddot{\theta} + \mathbf{W}_\theta \dot{\theta}^2 + \mathbf{V}_\theta \dot{\theta} + \Lambda_3 |\dot{\theta}| \dot{\theta} + \mathbf{K_{Dz}} \mathbf{f_{Dz}} + \mathbf{K_{Dy}} \mathbf{f_{Dy}} = \mathbf{D}^T \mathbf{u}, \qquad (41)$$

where $\mathbf{M}_\theta$, $\mathbf{W}_\theta$, $\mathbf{V}_\theta$, $\mathbf{K_{Dz}}$ and $\mathbf{K_{Dy}}$ are defined as

$$\mathbf{M}_\theta = \mathbf{J} + ml^2 \mathbf{S}_\theta \mathbf{V} \mathbf{S}_\theta + ml^2 \mathbf{C}_\theta \mathbf{V} \mathbf{C}_\theta + \Lambda_1 + l^2 \mu_n \mathbf{K}_1 \mathbf{K}^T \mathbf{S}_\theta + l^2 \mu_n \mathbf{K}_2 \mathbf{K}^T \mathbf{C}_\theta \qquad (42)$$

$$\mathbf{W}_\theta = ml^2 \mathbf{S}_\theta \mathbf{V} \mathbf{C}_\theta - ml^2 \mathbf{C}_\theta \mathbf{V} \mathbf{S}_\theta + l^2 \mu_n \mathbf{K}_1 \mathbf{K}^T \mathbf{C}_\theta - l^2 \mu_n \mathbf{K}_2 \mathbf{K}^T \mathbf{S}_\theta \qquad (43)$$

$$\mathbf{V}_\theta = \Lambda_2 - l\mu_n \mathbf{K}_2 \mathbf{V}_z^a - l\mu_n \mathbf{K}_1 \mathbf{V}_y^a \qquad (44)$$

$$\mathbf{K_{Dz}} = l\mu_n m_{11} A_1 \mathbf{ee}^T - l\mu_n m_{21} A_2 \mathbf{ee}^T - l\mathbf{S}_\theta \mathbf{K} \qquad (45)$$

$$\mathbf{K_{Dy}} = l\mu_n m_{12} A_1 \mathbf{ee}^T - l\mu_n m_{22} A_2 \mathbf{ee}^T + l\mathbf{C}_\theta \mathbf{K} \qquad (46)$$

where $\mathbf{K}_1 = A_1 + \mu_n A_1 \mathbf{ee}^T (m_{12} \mathbf{S}_\theta \mathbf{C}_\theta - m_{11} \mathbf{S}_\theta^2) - \mu_n A_2 \mathbf{ee}^T (m_{22} \mathbf{S}_\theta \mathbf{C}_\theta - m_{21} \mathbf{S}_\theta^2)$, $\mathbf{K}_2 = A_2 - \mu_n A_1 \mathbf{ee}^T (m_{11} \mathbf{S}_\theta \mathbf{C}_\theta - m_{12} \mathbf{C}_\theta^2) + \mu_n A_2 \mathbf{ee}^T (m_{21} \mathbf{S}_\theta \mathbf{C}_\theta - m_{22} \mathbf{C}_\theta^2)$, $A_1 = \mathbf{S}_\theta \mathbf{K} \mathbf{S}_\theta^2 + \mathbf{C}_\theta \mathbf{K} \mathbf{S}_\theta \mathbf{C}_\theta$, $A_2 = \mathbf{S}_\theta \mathbf{K} \mathbf{S}_\theta \mathbf{C}_\theta + \mathbf{C}_\theta \mathbf{K} \mathbf{C}_\theta^2$.

Remark 5. The model (35,41) has been adjusted compared to the model in [13] by redefining the expression of the link accelerations as in (9) in order to avoid a singularity issue of the model presented in [13].

The equations of motion for the underwater snake robot are in other words given by (35) and (41). By introducing the state variable $\mathbf{x} = \left[\theta^T, \mathbf{p}_{CM}^T, \dot{\theta}^T, \dot{\mathbf{p}}_{CM}^T\right]^T \in \mathbb{R}^{2n+4}$, we can rewrite the model of the underwater snake like robot compactly in state space form as

$$\dot{\mathbf{x}} = \left[\dot{\theta}^T, \dot{\mathbf{p}}_{CM}^T, \ddot{\theta}^T, \ddot{\mathbf{p}}_{CM}^T\right]^T = \mathbf{F}(\mathbf{x}, \mathbf{u}) \qquad (47)$$

where the elements of $\mathbf{F}(\mathbf{x}, \mathbf{u})$ are easily found by solving (35) and (41) for $\ddot{\mathbf{p}}_{CM}$ and $\ddot{\theta}$, respectively.

Remark 5. It is interesting to note that if, in the dynamic model (35) and (41), we change the axis z with x and set the hydrostatic forces to zero, then the model reduces to an identical hydrodynamic model of an underwater snake robot moving in a virtual horizontal plane, described in [13]. The underwater snake robot moving in a 2D plane of 3D is thus an extension of the underwater snake robot moving in a virtual horizontal plane.

III. SIMULATION RESULTS

In this section, simulation results are presented for three different modeling approaches: **case 1**–Added mass and nonlinear drag effect, **case 2**–Added mass, linear and nonlinear drag effect and **case 3**–Added mass, linear, nonlinear

drag and current effects. In the following, the mathematical expressions for lateral undulation and eel-like motion are presented. The models are implemented in *Matlab R2013b* on a laptop running MAC OS X Lion 10.7.5, 2.4 GHz Intel Core i7. The dynamics is calculated using the *ode23tb* solver with a relative and absolute error tolerance of 10^{-4}.

A. Lateral undulation

The gait pattern lateral undulation [1] is the fastest and most common form of snake locomotion. In order to achieve lateral undulation, the snake is commanded to follow the serpenoid curve [3]. The proposed lateral undulation is realized by controlling each joint of the snake robot according to the sinusoidal reference

$$\phi_i^* = \alpha \sin(\omega t + (i-1)\beta) + \gamma, \quad i = 1, \ldots, n-1, \quad (48)$$

where the parameters α and ω correspond to the amplitude and angular frequency of the sinusoidal joint motion, β determines the phase shift between the sequential joints, and γ is the joint offset that is used to control the direction of the motion.

B. Eel-like motion

Eel-like motion is achieved by propagating lateral axial undulations with increasing amplitude from nose to tail [27]. A simple equation is derived for the eel-like motion by controlling each joint of the snake robot according to the reference signal

$$\phi_i^* = \alpha \left(\frac{n-i}{n+1}\right) \sin(\omega t + (i-1)\beta) + \gamma, \quad i = 1, \ldots, n-1, \quad (49)$$

where the parameter $\alpha(n-i)/(n+1)$ corresponds to the increasing amplitude, from nose to tail, of the wave that propagates along the body of the snake robot.

C. Low-level joint control

A PD controller is used to calculate the actuator torques of the joints from their reference angles according to

$$u_i = \ddot{\phi}_i^* + k_d(\dot{\phi}_i^* - \dot{\phi}_i) + k_p(\phi_i^* - \phi_i), \quad i = 1, \ldots, n-1, \quad (50)$$

where $k_p > 0$ and $k_d > 0$ are the gains of the controller. During lateral undulation (48) and eel-like motion (49), we can easily calculate $\ddot{\phi}_i^*$ and $\dot{\phi}_i^*$, if γ is assumed to be a constant offset [1].

D. Simulation parameters

A snake robot was considered with $n = 10$ links, each one having length $2l = 0.14$ m and mass $m = \rho_b V$ kg. Three different values for the density of the snake robot are examined, $\rho_b = (1000, 998, 1002) \text{kg/m}^3$. The initial values of the states of the underwater snake robot were set to zero, i.e. the snake robot is initially at rest at the origin, with its heading along the inertial z axis. The hydrodynamic related parameters, $\hat{C}_D, \hat{C}_A, \lambda_1, \lambda_2, \lambda_3$, for the elliptic section with half small and great axis' length 0.03 m and 0.05 m, respectively, $\rho = 1000 \text{ kg/m}^3$, $C_f = 0.03$, $C_D = 2$, $C_A = 1$ and $C_M = 1$ were calculated using (12), (13), (15) and (17), respectively. Additionally, the anisotropic friction property is achieved by a low drag coefficient in the tangential direction and a higher one in the perpendicular. The values of a constant irrotational current in the inertial frame are set to $[0.1, 0.1]$ m/sec. In this simulation a joint PD controller (50) is used with parameters $k_p = 200, k_d = 50$, while lateral undulation or

eel-like motion are achieved by moving the joints according to (48) or (49), respectively, with gait parameters $\alpha = 30^o$, $\beta = 50^o$, $\omega = 70^o/\text{sec}$ and $\gamma = 0^o$.
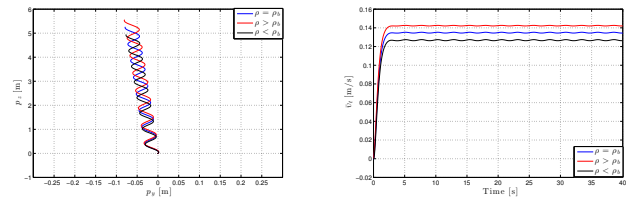
E. Lateral undulation: simulation results

In this section, simulation results for lateral undulation of the underwater snake robot are presented for the three different cases. In particular, the motion of the center of mass is presented in Fig. 4a-6a and the forward velocity (5) is presented in Fig. 4b-6b. All the simulation results are presented in case that a) the density of the robot is less than the density of the water, b) for neutrally buoyant robot and c) for the case where the density of the body is greater than the density of the water. These cases are examined in order to investigate the total motion response of a not neutrally buoyant underwater snake robot considering three different modeling approaches. From the simulation results we can conclude that small variations between ρ_b and ρ have a negligible effect in the total motion response of the underwater snake robot, in the case where the detailed modeling of the hydrodynamic effects is considered (Fig.6a-6b). This indicates that the modeling with detailed modeling of the hydrodynamic effects is less sensitive in variation between the density of the water and the density of the body. However, in case 1, where only the added mass and linear drag effects are considered, it is shown that even small variation between the densities has significant effects in the overall motion (Fig. 4a-4b).
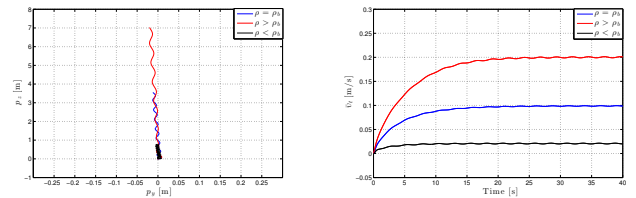
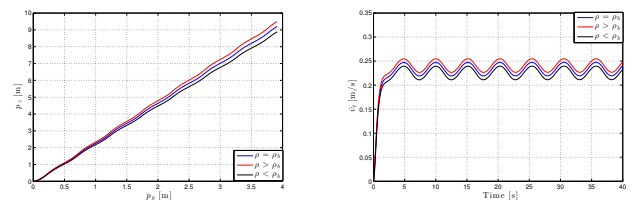(a) Position of the CM   (b) Velocity of the CM

Fig. 4: Case 1: Simulation results for lateral undulation: Computational time=$\{26.66, 26.67, 29.23\}$ sec

(a) Position of the CM   (b) Velocity of the CM

Fig. 5: Case 2: Simulation results for lateral undulation: Computational time=$\{26.33, 28.46, 28.52\}$ sec

(a) Position of the CM   (b) Velocity of the CM

Fig. 6: Case 3: Simulation results for lateral undulation: Computational time=$\{28.63, 28.20, 28.14\}$ sec

F. Eel-like motion: simulation results

In this section, we present and compare the simulation results for the eel-like motion pattern for the three different modeling approaches. In particular, the motion of the center of mass is presented in Fig. 7a-9a and the forward velocity is presented in Fig. 7b-9b. When $\rho < \rho_b$, the robot moves backwards (Fig. 7a-7b) and this happens because the robot did not manage to achieve positive forward propulsion for the chosen parameters of eel-like motion. However, it can be easily seen that the effects of error between the ρ and ρ_b vanish in Fig. 9a-9b.
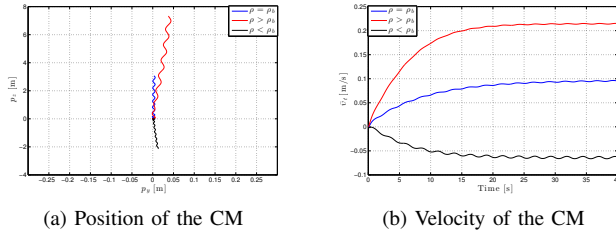

(a) Position of the CM   (b) Velocity of the CM

Fig. 7: Case 1: Simulation results for eel-like motion: Computational time=$\{20.45, 20.57, 20.55\}$ sec

(a) Position of the CM   (b) Velocity of the CM
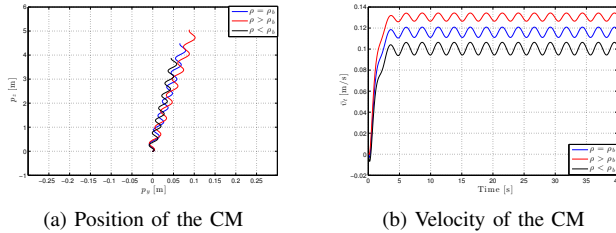
Fig. 8: Case 2: Simulation results for eel-like motion: Computational time=$\{19.24, 20.14, 19.14\}$ sec

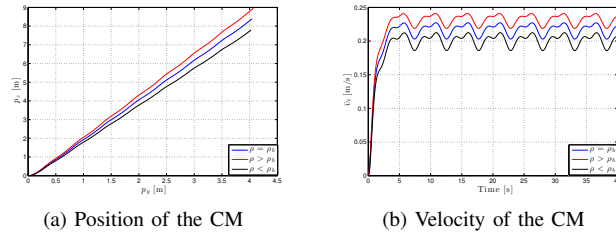(a) Position of the CM   (b) Velocity of the CM

Fig. 9: Case 3: Simulation results for eel-like motion: Computational time=$\{19.98, 19.89, 20.10\}$ sec

IV. CONCLUSIONS AND FUTURE WORK

This paper has presented a model of the kinematics and dynamics of an underwater snake robot moving in a 2D tilted vertical plane of 3D. The model is in closed-loop form and is thus particularly well suited for model-based control design schemes. In this modeling approach, the combination of linear and nonlinear drag forces, the added mass effect, the fluid moments and current effect are considered. In addition, this modeling approach takes into account the hydrostatic forces due to the buoyancy and gravity. Simulation results for lateral undulation and eel-like motion are presented. In future work, the authors will employ the proposed model, in order to develop and analyze controllers for underwater snake robots.

REFERENCES

[1] P. Liljebäck, K. Pettersen, Ø. Stavdahl, and J. T. Gravdahl, *Snake Robots: Modelling, Mechatronics, and Control*, Springer-Verlag, Ed. Advances in Industrial Control, 2013.

[2] J. Gray, "Studies in animal locomotion," *Journal of Experimental Biology*, vol. 10, no. 1, pp. 88–104, 1933.

[3] S. Hirose, *Biologically Inspired Robots: Snake-Like Locomotors and Manipulators*. Oxford: Oxford University Press, 1993.

[4] A. Crespi, A. Badertscher, A. Guignard, and A. Ijspeert, "Swimming and crawling with an amphibious snake robot," in *Proc. of the IEEE International Conference on Robotics and Automation*, April 2005, pp. 3024 – 3028.

[5] F. Boyer, D. Chablat, P. Lemoine, and P. Wenger, "The eel-like robot," *CoRR*, vol. abs/0908.4464, 2009.

[6] H. Yamada, S. Chigisaki, M. Mori, K.Takita, K. Ogami, and S. Hirose, "Development of amphibious snake-like robot ACM-R5," in *Proc. 36th Int. Symp. Robotics*, 2005.

[7] K. McIsaac and J. Ostrowski, "Motion planning for anguilliform locomotion," *IEEE Trans. Rob. Aut.*, vol. 19, no. 4, pp. 637–625, 2003.

[8] F. Boyer, M. Porez, and W. Khalil, "Macro-continuous computed torque algorithm for a three-dimensional eel-like robot," *IEEE Transactions on Robotics*, vol. 22, no. 4, pp. 763 –775, Aug. 2006.

[9] A. Wiens and M. Nahon, "Optimally efficient swimming in hyper-redundant mechanisms: control, design, and energy recovery." *Bioinspir Biomim*, vol. 7, no. 4, 2012.

[10] G. Taylor, "Analysis of the swimming of long and narrow animals," *Proc. of the Royal Society of London. Series A. Mathematical and Physical Sciences*, vol. 214, no. 1117, pp. 158–183, 1952.

[11] M. J. Lighthill, "Large-amplitude elongated-body theory of fish locomotion," *Proc. of the Royal Society of London. Series B. Biological Sciences*, vol. 179, no. 1055, pp. 125–138, 1971.

[12] J. Chen, W. O. Friesen, and T. Iwasaki, "Mechanisms underlying rhythmic locomotion: body-fluid interaction in undulatory swimming," *The Journal of Experimental Biology*, vol. 214, no. 4, pp. 561–574, 2011.

[13] E. Kelasidi, K. Y. Pettersen, J. T. Gravdahl, and P. Liljebäck, "Modeling of underwater snake robots," in *Proc. of IEEE International Conference on Robotics and Automation*, Hong Kong, China, May 31 - June 7 2014.

[14] J. Blair and T. Iwasaki, "Optimal gaits for mechanical rectifier systems," *IEEE Transactions on Automatic Control*, vol. 56, no. 1, pp. 59–71, 2011.

[15] F. Candelier, M. Porez, and F. Boyer, "Note on the swimming of an elongated body in a non-uniform flow," *Journal of Fluid Mechanics*, vol. 716, pp. 616–637, 2013.

[16] F. Boyer, M. Porez, A. Leroyer, and M. Visonneau, "Fast dynamics of an eel-like robot-comparisons with navier-stokes simulations," *IEEE Transactions on Robotics*, vol. 24, no. 6, pp. 1274–1288, 2008.

[17] O. Ekeberg, "A combined neuronal and mechanical model of fish swimming," *Biological Cybernetics*, vol. 69, pp. 363–374, 1993.

[18] W. Khalil, G. Gallot, and F. Boyer, "Dynamic modeling and simulation of a 3-d serial eel-like robot," *IEEE Transactions on Systems, Man, and Cybernetics, Part C: Applications and Reviews*, vol. 37, no. 6, pp. 1259 –1268, Nov. 2007.

[19] L. Zhu, Z. Chen, and T. Iwasaki, "Oscillation, orientation, and locomotion of underactuated multilink mechanical systems," *IEEE Transactions on Control Systems Technology*, vol. 21, no. 5, pp. 1537–1548, 2013.

[20] J. Morison, J. Johnson, and S. Schaaf, "The force exerted by surface waves on piles," *Journal of Petroleum Technology*, vol. 2, pp. 149–154, May 1950.

[21] W. Khalil, G. Gallot, O. Ibrahim, and F. Boyer, "Dynamic modeling of a 3-d serial eel-like robot," in *Proc. of the IEEE International Conference on Robotics and Automation*, April 2005, pp. 1270 – 1275.

[22] S. Fan and C. Woolsey, "Underwater vehicle control and estimation in nonuniform currents," in *Proc. American Control Conference*, Washington, DC, June 17-19 2013.

[23] T. I. Fossen, *Handbook of Marine Craft Hydrodynamics and Motion Control*. John Wiley & Sons, Ltd, 2011.

[24] J. Newman, *Marine Hydrodynamics*. MIT Press, 1977.

[25] F. White, *Fluid Mechanics*. McGraw-Hill series in mechanical engineering, McGraw-Hill Higher Education, 2003.

[26] J. J. Myers, C. Halm, and R. McAllister, *Handbook of Ocean and Underwater Engineering*. McGraw Hill, New York, 1969.

[27] J. Colgate and K. Lynch, "Mechanics and control of swimming: a review," *IEEE Journal of Oceanic Engineering*, vol. 29, no. 3, pp. 660 – 673, July 2004.